Regular Article

PHYSICAL CHEMISTRY RESEARCH
Published by the
Iranian Chemical Society
www.physchemres.org
info@physchemres.org

Phys. Chem. Res., Vol. 9, No. 4, 701-713, December 2021
DOI: 10.22036/PCR.2021.272919.1886

DFT Studies on Molecular Structure, Absorption properties, NBO Analysis, and Hirshfeld Surface Analysis of Iron(III) Porphyrin Complex

S. Dhifaoui[a,*], A. Azaid[b], M. Bourass[c], L. Ben Haj Hassen[a], H. Nasri[a] and M. Bouachrine[b,d,*]

[a]*Laboratoire de Physico-chimie des Matériaux, Université de Monastir, Faculté des Sciences de Monastir, Avenue of the Environment, 5019 Monastir, Tunisia*

[b]*Molecular Chemistry and Natural Substances Laboratory, Faculty of Sciences, University Moulay Ismail, BP–11201 Zitoune, Meknes, Morocco*

[c]*Institut des Sciences Moléculaires, Université de Bordeaux, UMR 5255 CNRS 351 cours de la Libration, 33405 Talence (France)*

[d]*EST Khenifra, Université Sultan Moulay Slimane, Khenifra, Morocco*

(Received 11 February 2021, Accepted 15 June 2021)

In this work, density-functional theory (DFT) calculations, natural bond orbital (NBO) analysis, and Hirshfeld surface analysis were carried out on the bis(4-cyanopyridine) [(*meso*-tetrakis(4-metoxyphenylporphyrinato)] iron(III) trifluoromethanesulfonate chlorobenzene mono-solvate complex(I). The structure of the ferric porphyrin derivative (I) was optimized using various quantum chemical methods and calculated using HF, B3PW91, BPV86, and B3LYP with three bases set: 3-21, 6-31G(d,p), and 6-311G(d,p). The theoretical structural parameters of (I) were very close to those obtained by X-ray molecular structure. From the optimized structure, several parameters, such as HOMO-LUMO energies, dipole moments, molecular electrostatic potentials, Mulliken electronegativity, chemical hardness, and electronic potential, were calculated and discussed. Furthermore, the absorption properties of (I) were obtained and compared with those obtained with the experimental UV-Vis spectrum. The reactivity of our $[Fe^{III}(TMPP)(4\text{-}CNpy)_2]^+$ ion complex was calculated using various descriptors, such as local softness, electrophilicity, electronegativity, hardness, HOMO-LUMO gap. Finally, the Hirshfeld data of the crystal packing of (I) were discussed.

Keywords: Iron(III) porphyrin complex, DFT calculation, Natural bond orbital (NBO) analysis, Absorption properties, Hirshfeld surface analysis

INTRODUCTION

Since the 1960s, iron(III) metalloporphyrins have been extensively used as models for hemoproteins due to their close resemblance to the active sites of hemoproteins, such as hemoglobin, myoglobin, cytochromes P450, and cytochromes c, storage and transport of oxygen, chlorophyll for photosynthesis, and different types of enzymes and vitamins [1-3]. Synthetic porphyrins and metalloporphyrins are widely applied not only in biology but also in chemistry, physics, and other fields of technology. In fact, large numbers of these iron species are used in catalysis, compound semiconductors, and photovoltaic materials. Furthermore, these porphyrin complexes have wide applications in the field of electronics and nonlinear optics (NLO); in fact, these compounds can function as second harmonic generators, frequency converters, and electro-optical modulators [5]. It is noteworthy that for hemoproteins, the relative orientation of the two histidine planes is correlated with several electronic, magnetic, and stereochemical properties of these iron biological systems, such as the reduction potentials [6]. To further understand the effects of the relative orientation on the above-mentioned properties of hemoproteins, numerous compounds of iron(III) hexa-coordinated metalloporphyrins

*Corresponding authors. E-mail: bouachrine@gmail.com; dhifaoui.salma@gmail.com

with parallel bis(N-donor) planar axial have been studied. This is the case of bis(imidazole), bis(substituted imidazoles), bis(pyridine), and bis(substituted pyridines) ferric porphyrin complexes [7]. Recently, to further investigate the properties of iron(III) hexa-coordinated complexes bearing neutral N-donor trans-planar axial ligands, Haj Hassen *et al.* reported synthesis, spectroscopic, magnetic, and electrochemical data and the X-ray molecular structure of the bis(4-cyanopyridine) [(*meso*-tetrakis(4-metoxyphenylporphyrinato)] iron(III) trifluoromethane-sulfonate chlorobenzene mono-solvate complex with the formula $[Fe^{III}(TMPP)(4\text{-}CNpy)_2]SO_3CF_3.C_6H_5Cl$ [8]. The present study is a theoretical study using density functional theory (DFT) calculations of the structural and spectroscopic properties of the $[Fe^{III}(TMPP)(4\text{-}CNpy)_2]^+$ ion complex to compare the theoretical results of this study with those of experimental studies already conducted and to calculate other parameters that can shed light on possible new applications of this coordination compound. The purpose of DFT calculations in this study was to, first, calculate the energies of the highest occupied molecular orbital-lowest unoccupied molecular orbital (HOMO-LUMO) and, secondly, calculate the gap energy. Then, the results were used to calculate several parameters, such as the electric dipole moment (μD), hyperpolarizability (βtot), molecular electrostatic potential (MEP), and the natural bond orbital (NBO). The theoretical UV-Vis properties of $[Fe^{III}(TMPP)(4\text{-}CNpy)_2]^+$ were also investigated.

Finally, the results of Hirshfeld surface analysis and molecular structure of the $[FeIII(TMPP)(4\text{-}CNpy)_2]^+$ ion complex were investigated and compared with those obtained by single-crystal X-ray diffraction [8].

EXPERIMENTAL

Hirshfeld Surface Analysis

Hirshfeld surfaces [9,10] and the related fingerprint plots (2D) [11] were created using Crystal Explorer 3.1 [12]. The input files were utilized based on the results of single-crystal X-ray diffraction studies. Hirshfeld surfaces and their 2D fingerprint plots have been used to show intermolecular interactions [13]. Dnorm is based on the sum of both 'di' and "de", which are normalized by the Van der Waals radius of the atom. The parameter 'di' is the distance from the nearest nucleus interior to the surface while the parameter 'de' is the external contact. Dnorm reflects intermolecular distances using a red-white-blue color scheme, in which red is used for shorter contacts, blue for longer contacts, and white for contacts around the vdW separation. A 2D fingerprint plot resulted from the combination of de and di presents a summary of intermolecular contacts in the crystal.

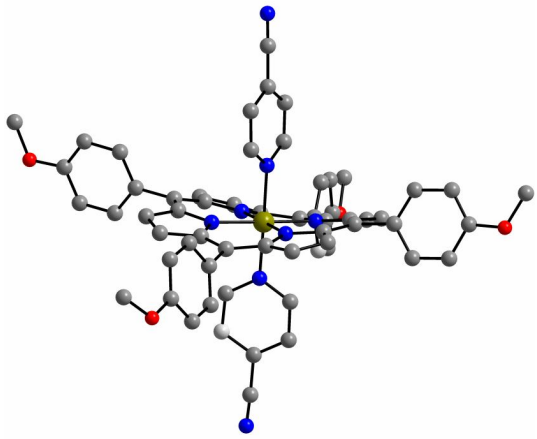

Fig. 1. The iron complex of $[Fe^{III}(TMPP)(4\text{-}CNpy)_2]^+$. The hydrogen atoms are omitted for clarity.

$$d_{norm} = \frac{d_i - r_i^{vdw}}{r_i^{vdw}} + \frac{d_e - r_e^{vdw}}{r_e^{vdw}} \quad (1)$$

Computational Methods

The quantum chemical calculations were carried out using the DFT/B3LYP/6-311G(d,p) method [14-15]. From the obtained optimized structures, we examined the HOMO, LUMO, and E_{gap} to predict the localization of electronic populations and electronic structures. All calculations were carried out using the GAUSSIAN 09 program [16]. The absorption and emission spectra and the oscillator strengths were investigated using the TD-CAM-B3LYP method on fully optimized geometries [17].

RESULTS AND DISCUSSION

X-Ray Crystal Structures

The experimental structural analysis of the studied complex $C_{67}H_{49}ClF_3FeN_8O_7S$ was previously reported by Haj Hassen *et al.* [8] (Fig. 1). Their analysis indicated that

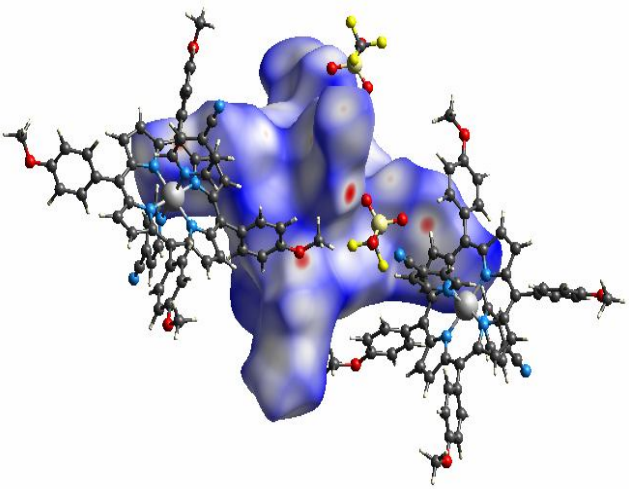

Fig. 2. Hirshfeld surfaces mapped with dnorm for the title compound.

the majority of distances and binding angles were in the standards. The Fe-N distances varied from 1.949 to 2.001 Å, and the bonding distances were as follows: Fe-N1 = 1.969(2) Å, Fe-N2 = 1.976(2) Å, Fe-N3 = 1.969(2) Å, Fe-N4 = 1.969(2) Å, Fe-N7 = 2.008(2) Å, Fe-N8 = 2.005(2) Å. In the 4-cyanopyridine, the N-C distances ranged from 1.344(4) Å to 1.351(4) Å, and the C-C distances were about 1.383. The binding angles involving Iron and other atoms ranged from 98.99-179°. The crystal packing was stabilized into a three-dimensional network by hydrogen and π-π interactions, as illustrated below.

Hirshfeld Surfaces Analysis

The Hirshfeld surfaces and fingerprint graphics are illustrated in Figs. 2 and 3. In these Hirshfeld surfaces, the red spots indicate the presence of close contacts whereas

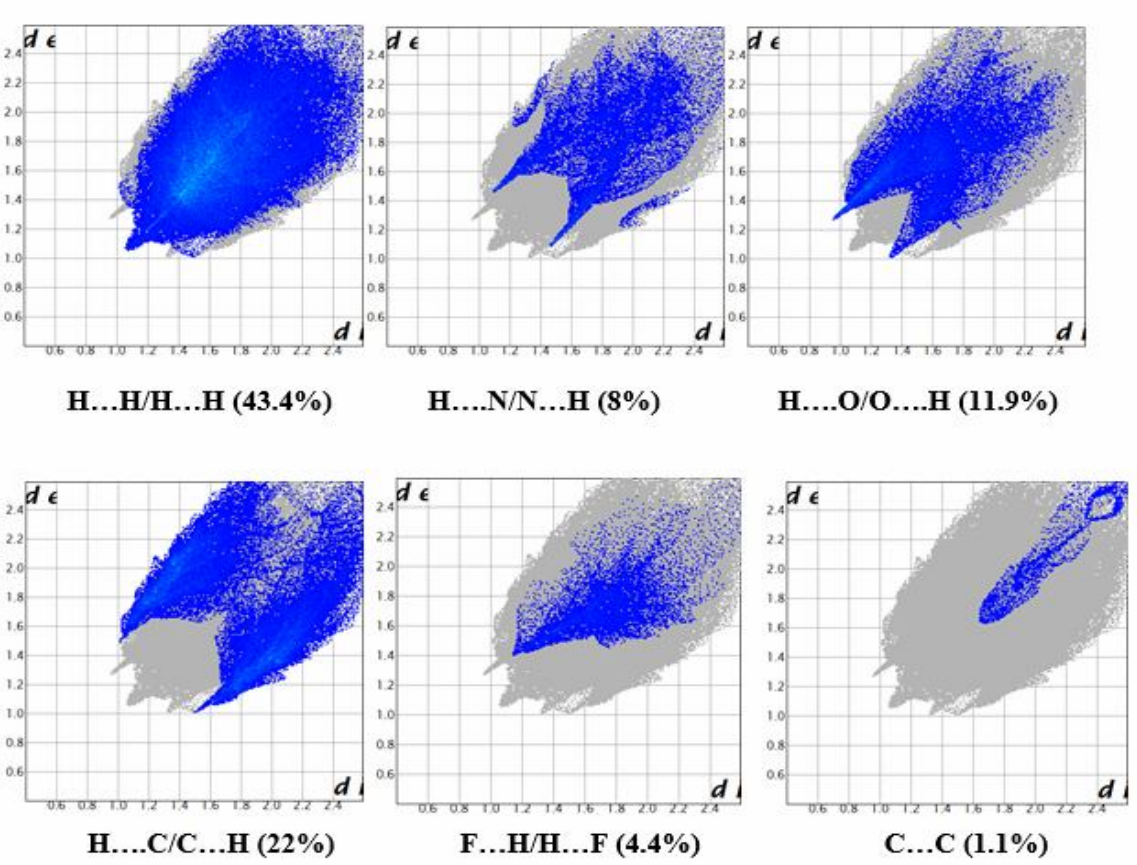

Fig. 3. Fingerprint plots: full and resolved into different dominant intermolecular interactions within the studied complex, showing percentages of contacts contributed to the total Hirshfeld surface area.

areas without close contacts are visualized as blue spots. The crystal packing of porphyrin is mainly controlled by the close contacts involving Carbon (C…H–O), which are observed as intense red spots on the Hirshfeld surfaces. The H–O contacts occupied 11.9% of the total fingerprint, with a minimum value of (de + di) around 2.41 Å. In the crystal, 43.4% of the intermolecular contacts were associated with H-H contacts, 22% with the contacts between carbon and hydrogen C–H, 8% with the N–H contacts, and 1.1% with the π-π stacking (C…C). These results also confirm the H–A distances corresponding to these interactions [8].

Molecular Geometry

First, we performed a preliminary study by optimizing the structure of the studied molecule using numerous quantum chemistry methods, including HF, B3PW91, BPV86, and B3LYP with three bases set: 3-21, 6-31G(d,p), and 6-311G(d,p). Then, we determined the structural parameters (distances and angles) from the optimized geometries obtained by several methods (Fig. 4). The results showed that the B3LYP method with the base 6-311G(d,p) was the most accurate method, making it possible to reproduce with negligible errors in the experiment. It should be noted that these slight errors are related to the fact that the calculation results belong to the gaseous phase while the experimental properties belong to a solid state. Thus, we adopted the above-mentioned method for the rest of this study. Some structural parameters calculated with B3LYP/6-311G(d,p) are presented in Table 1. The structural properties obtained experimentally in the section X-Ray Crystal were compared with the optimized structural parameters, such as bond length and bond angle, and the results are presented in Table 1. The values of the bond lengths of the C–C ring calculated in the gaseous phase ranged from 1.39290-1.51058 Å while the experimental bond lengths ranged from 1.371(3) to 1.510(4). The lengths of the N–C and C–O bonds were calculated at 1.47550 and 1.68240 Å, respectively, and the corresponding experimental values were 1.475(3) and 1.6203, respectively (16). The observed Fe-N bond lengths were at 1.219(2) and 1.219(2) Å while the calculated values were at 1.23266 and 1.22474 Å. Slight differences were observed in the structural parameters when the X-ray structure of bis(4-cyanopyridine) [(*meso*-tetrakis(4-metoxyphenyl-porphyrinato)] iron(III) trifluoromethanesulfonate chlorobenzene mono-solvate was compared to that obtained after optimization. This can be explained by the fact that in the solid state, there is a crystalline field that favors

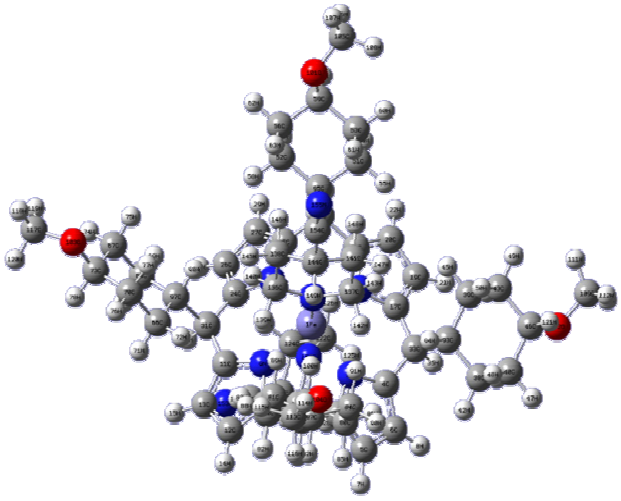

Fig. 4. The B3LYP/6-311G(d,p) optimized geometries of the studied compounds.

Table 1. Geometrical Parameters of the Studied Complex

Bond lengths (Å)	Exp.	Bond angles (°)	Exp.
Fe–N1	1.969(2)	N1–Fe–N3	178.92(10)
Fe–N2	1.976(2)	N2–Fe–N8	89.35(9)
Fe–N3	1.969(2)	N2–Fe–N7	90.39(9)
Fe–N4	1.969(2)	N1–Fe–N7	88.55(10)
Fe–N7	2.008(2)	N1–Fe–N8	89.80(10)
Fe–N8	2.005(2)	N8–Fe–N7	178.33(11)
N5–C33	1.141(4)	N5–C33–C30	177.3(4)
N6–C39	1.140(5)	N6–C39–C36	179.3(5)
C46–C51	1.377(4)	C46–C51–C50	121.7(3)
C47–C48	1.377(5)	C47–C48–C49	120.3(3)
N7–C32	1.344(4)	N7–C32–C31	123.1(3)
N8–C38	1.351(4)	N8–C38–C37	122.5(3)

Table 2. B3LYP/6-311g(d,p) Calculated Values of μ, α and β

Parameters	Calculated values	Parameters	Calculated values
m_x	-2.1502	Bxxx	51.3155
m_y	-0.8134	Byyy	-134.7982
m_z	0.4618	Bzzz	-15.9148
m_{tot} (D)	2.3448	Bxxy	-89.0946
a_{xx}	28.804	Bxxz	-73.8417
a_{yy}	-72.842	Bxyy	-234.5659
a_{zz}	44.037	Bxzz	-30.2863
a_{xy}	-15.129	Bxyz	-51.5900
a_{xz}	8.303	Byzz	-68.2126
a_{yz}	-11.708	Byyz	55.1727
a_0 (a.u.)	-0.301	btot (esu)	31.4831×10^{-31}
Da (a.u.)	7765,279		

intermolecular interactions whereas in quantum chemistry calculations, it is assumed that the state is gaseous.

Hyperpolarizability Calculation

Nonlinear optical (NLO) properties are currently of considerable importance and have been the subject of much research in the field of communication technology, signal processing, optical interconnections, optical memory, and optical modulation [18]. NLO properties are one of the futures of emerging technology in areas such as telecommunications, signal processing, and optical interconnections [19-20]. As regards NLO properties, the nonlinear optical response of an isolated molecule in an electric field E_i (x) can be represented by a Taylor series development of the total dipole moment (μ_{tot}) induced by the field [21].

$$\mu_{tot} = \mu_0 + \alpha_{ij}E_j + \beta_{ijk}E_{jk} + \ldots$$

The first hyperpolarizability (β_0) of this molecular system was calculated using HF and B3LYP/6-31G(d,p) method, based on the finite field approach (Table 2). The complete equations used to calculate the magnitude of the total static dipole moment (μ), the mean Polarizability (α_0), the anisotropy of the polarizability (Δα), and the mean first polarizability (β_0), using the x, y, z components obtained by the Gaussian 03 W program, are as follows:

$$\mu_{tot} = (\mu_x^2 + \mu_y^2 + \mu_z^2)^{1/2}$$

$$\alpha_0 = 1/3\ (\alpha_{xx} + \alpha_{yy} + \alpha_{zz})$$

$$\Delta\alpha = 2^{-1/2}\ ((\alpha_{xx} - \alpha_{yy})^2 + (\alpha_{yy} - \alpha_{zz})^2 + (\alpha_{xx} - \alpha_{zz})^2 6\alpha_{xx}^2)^{1/2}$$

$$\beta x = \beta xxx + \beta xyy + \beta xzz$$

$$\beta y = \beta yyy + \beta yxx + \beta yzz$$

$$\beta z = \beta zzz + \beta zxx + \beta zyy$$

$$\beta_{tot} = (\beta x^2 + \beta y^2 + \beta z^2)^{1/2}$$

Since the calculated values of polarizability and hyperpolarizability were in atomic units (au), they were converted to electrostatic units (esu) for α as 1 ua = 0.1482×10^{-24} esu and for β as 1 ua = 8.6393×10^{-33} esu.

The prototype urea molecule is used in research to study the NLO properties of molecular compounds; its hyperpolarizability value is widely used as a threshold value to be compared with other candidate molecules. The calculated first hyperpolarizability of the studied molecule was 31.4831×10^{-31} esu, which is four times higher than that

HOMO LUMO

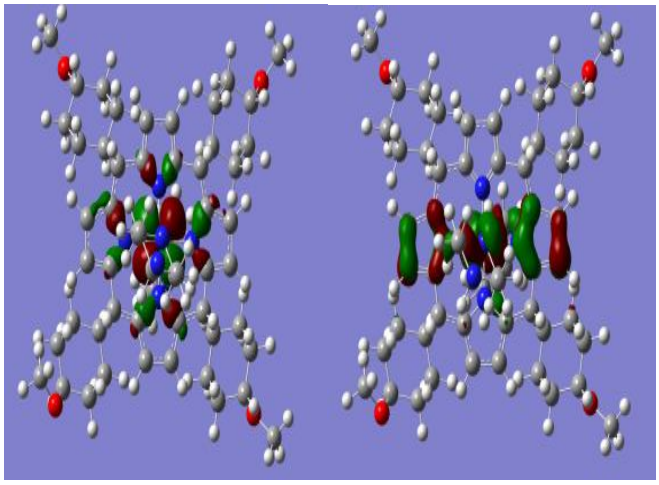

Fig. 5. The density plots of the HOMO and LUMO frontier orbitals of the studied compound calculated at the B3LYP/6-311(d,p) level.

of urea (7.7289×10^{-31} esu). Thus, it can be stated the studied complex may serve as a promising building block for NLO materials.

Electronic Properties

To obtain some information regarding the electronic properties, distribution patterns, and densities of the frontier molecular orbitals (FMOs), we examined the HOMO and LUMO levels. The relative order of these orbitals provided us with some information on intramolecular charge transfer/transport (ICT) [22-23]. As a result, and as indicated in Fig. 5, the HOMO and LUMO orbitals were located on the center of the complex, especially around the aromatic cycles surrounding the metal. The increased electron density in this region can be attributed to the excess nitrogen and the extended length of π-conjugation. We also noticed that HOMO orbitals had an antibonding character between consecutive subunits while the LUMO orbitals had a binding character between consecutive subunits.

The HOMO and LUMO frontier orbitals are very important parameters that provide information on the chemical reactivity of many organic molecules [24-25]. It should be noted that the HOMO orbital acts mainly as an electron donor whereas the LUMO orbital acts largely as an electron acceptor, and the gap between HOMO and LUMO, called the "HOMO-LUMO gap", characterizes the chemical stability.

The frontier orbitals of the studied compounds are plotted in Fig. 6. The molecular orbital calculations indicated that the title compound had 30 occupied molecular orbitals. The HOMO-LUMO energy gap of 8C1M6PB was calculated at the DFT-B3LYP level using 6-311G(d,p), and the results are presented in Table 3.

The HOMO-LUMO energy gap values were calculated at 0.9042 eV in B3LYP/6-311G(d,p). The results showed that the studied molecule had a small value of band gap, which can be attributed to the improvement of the conjugation due to the presence of a two-conjugated system complexed with the metal.

The possibility of delocalization on the entire ligand has been intensively studied by many authors [26-27]. The results show that this delocalization depends on the electron donor or acceptor character of the chelating groups and the ligands surrounding the metal.

The Mulliken electronegativity (χ) [28], chemical hardness (η), and electronic potential (μ) were calculated using HOMO (E_{HOMO}) and LUMO (E_{LUMO}) orbital energies [29-30-31]. These parameters were calculated using Koopmans' theorem [32].

Electronegativity: $\chi = -\mu = -(E_{HOMO} + E_{LUMO})/2$

Chemical potential: $\mu = (E_{HOMO} + E_{LUMO})/2$

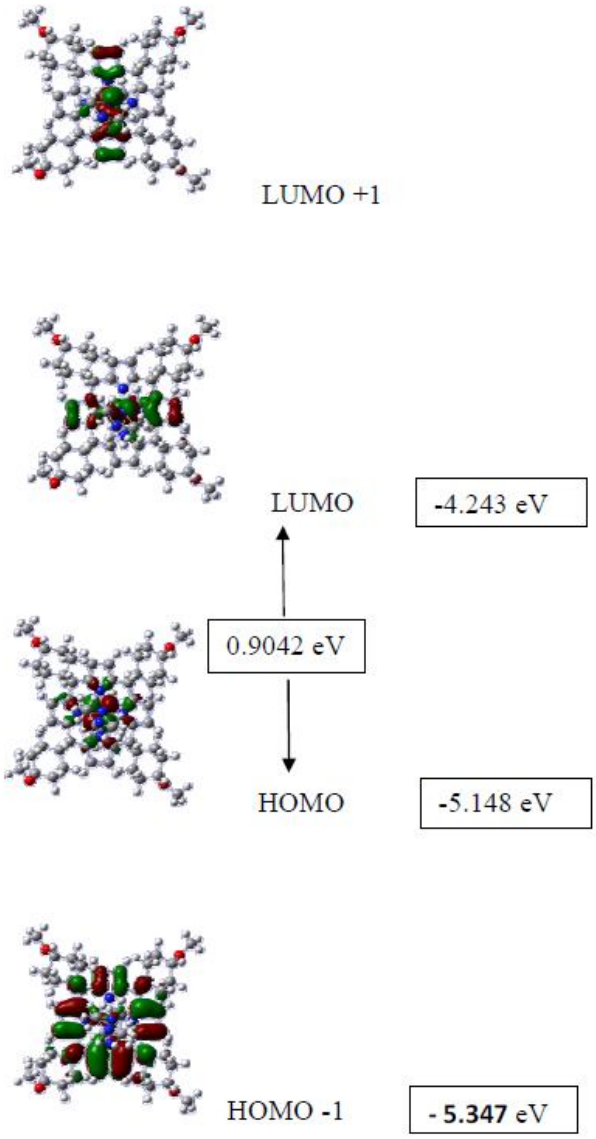

Fig. 6. The HOMO, LUMO, HOMO-1, and LUMO+1 orbitals of the studied compounds.

The chemical hardness η was defined similarly to express the resistance of a molecule to the exchange electron density with the environment [33-34].

$$\text{Chemical hardness: } \eta = (E_{LUMO} - E_{HOMO})/2$$

The electronic and optical properties are generally governed by the HOMO-LUMO energies and gap. They play an important role in understanding the reactivity and stability of organic molecules possessing a p-conjugate system. It should be added that the analysis of HOMO and LUMO orbitals also makes it possible to predict the most reactive sites. In addition, the energy gap (E_g) characterizes conjugated molecules and macromolecules and explains ICT along the conjugated molecular chain [22-23]. Therefore, electron density transfers from the conjugated part of the molecule in the donor site to the acceptor part.

Generally, organic molecules are divided into two types: hard molecules and soft molecules. Hard molecules are characterized by a large energy gap. However, the latter ones are characterized by a small energy gap, which is the case of our complex (0.9042 eV). The stability of molecules is closely related to their hardness, meaning that the molecules with higher energy gaps (*i.e.*, hard molecules) are less reactive. For this reason, several properties, including energy gap, HOMO energy, LUMO energy, and absorption wavelength (λ_{max}), were studied in the present study. The electronic and chemical properties obtained from the optimized structure, namely, the frontier energies (*i.e.*, E_{HOMO}, E_{LUMO}, and E_{gap}), the chemical potential, the global hardness, and electronegativity of the studied compound (M1), are presented in Table 3.

The following conclusions can be drawn from the results presented in Table 3:

Table 3. Electronic Properties (*i.e.*, HOMO, LUMO, and E Gap (eV)), Chemical Hardness (η), Chemical Potential (μ), and Electronegativity (χ) Obtained at the B3LYP/6-31G(d,p) Level for the Studied Compound

Compound	E_{HOMO}	E_{LUMO}	E_{gap} (eV)	μ (eV)	η (eV)	X (eV)
M1	-5.148	-4.243	0.9042	-4.6955	0.4525	4.6955

1- By considering the obtained values of the chemical potential and electronegativity of the complex and given that that the passage of electrons takes place in compounds with the highest chemical potential and lowest electronegativity, it can be concluded and confirmed that the studied complex will behave as an electron donor.
2- The studied molecule had low hardness values (0.4525 eV), so it can be concluded that it is a soft molecule. This is probably due to the low value of the energy gap in the studied molecule, suggesting that it may tend to have a facile rearrangement of its electronic structure and an interesting reactivity.

Molecular Electrostatic Potential

The polarity of the studied complex was determined by the MEP. This technique carefully describes physicochemical and, especially, electrostatic interactions within the molecule by providing basic information on the physicochemical properties of the molecule, such as the molecular size and shape, in the form of color change [26-27]. In fact, MEPs are presented in several colors. Most negative and positive potentials are presented by red and blue colors, respectively, whereas the green color indicates the neutral area. The MEP surface of the studied complex is shown in Fig. 7. We found that the region surrounding the metal was characterized by a red color, suggesting that this region had the most negative potential. However, the hydrogens linked to the chelating methoxyphenyl-porphoyrinato and 4-cyanopyridine groups represent the region with the most positive potentials and charge because this region is shown in blue color. Total electron density of the studied complex varied from -8.446 e^{-2} to + 8.44 e^{-2}.

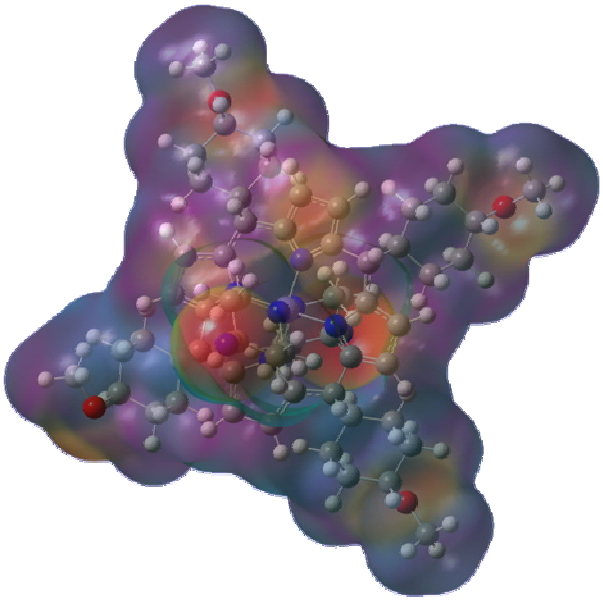

Fig. 7. MEP surface of the complex.

Absorption Properties

The electron spectra of the studied compound are shown in Fig. 8. The positions of the Soret and Q bands are as follows:
- 400 nm (Soret bands), mainly corresponding to the transition from the ground state S_0 to the second singlet state S_2 in the porphyrin ligands;
- 500 nm (Q bands), corresponding to the transition S0-S1;
- Other bands with long wavelengths (> 700 nm), probably preventing the overlaps with the OA t2g of the Fe metal.

It is worth noting that the conjugation in the porphyrin cycles results in strong absorption in the UV and the visible regions. The absorption spectrum in porphyrins shows bands in the vicinity of 400 nm (π-π* transition). It is important to mention that the redshift (Q bands) (500 nm) is mainly caused due to the presence of phenyl groups at the meso positions of the porphyrin, which, in turn, leads to a significant steric interaction between them [36]. That said, the value of the optical gap determined from the simulated absorption spectrum and obtained by the CAM-B3LYP method was 1.911 eV, which was close to the experimental value (1.71 eV) of the electron spectrum [8]. A comparison of these theoretical energy values with those obtained experimentally showed a slight difference. This slight difference can be explained by the fact that the theoretical calculations are supposed to be made in the gaseous state while the experimental values belong to the solid state.

Density of States

To determine the transport and photoelectric properties and better understand the behavior of semiconductors, electron and hole populations must be studied at the conduction and valence bands. To do this, the electronic density of states (EDOS) should be reported. This value, which depends on the electronic energy E, corresponds to

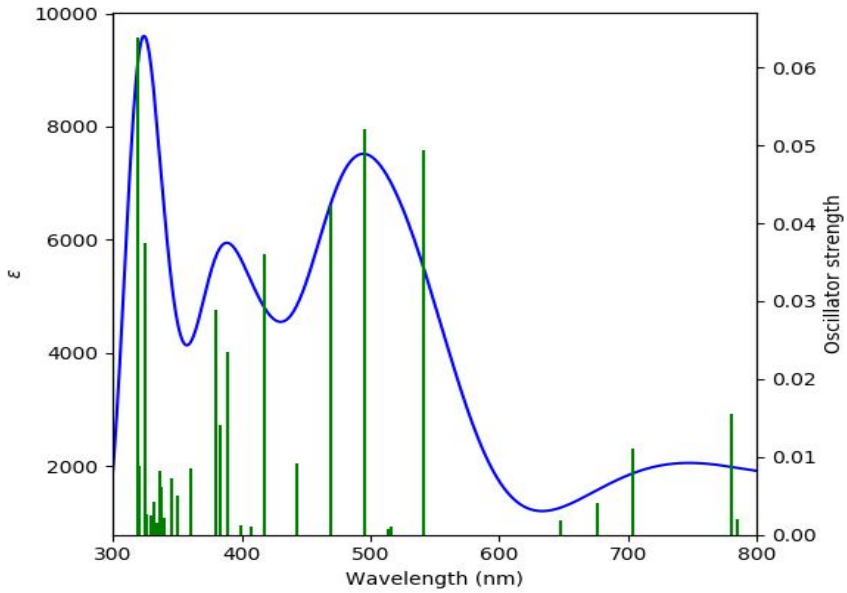

Fig. 8. Simulated UV-Vis optical absorption spectra of the studied complex obtained by the CAM/B3LYP method.

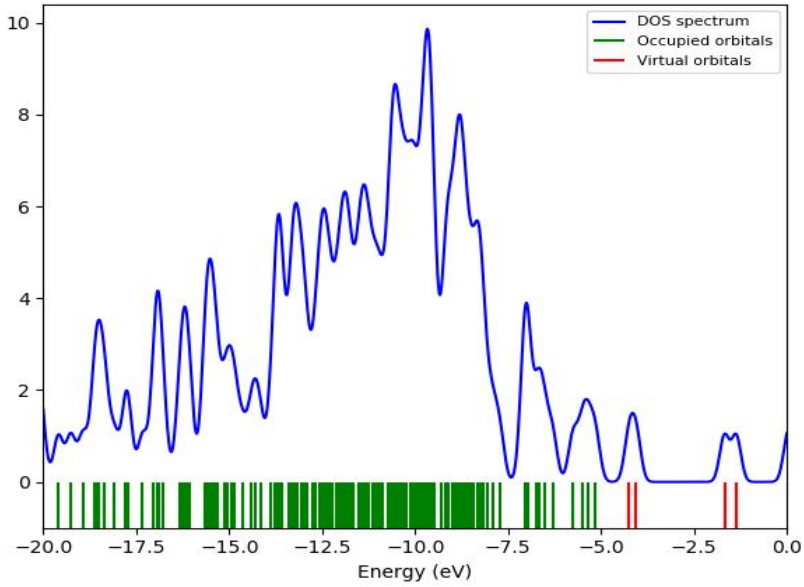

Fig. 9. The DOS spectrum of the studied complex based on DFT calculations.

the space available for the electrons in the conduction band and the place available for the holes in the valence band. It also has the advantage of quantifying the number of solid-state electronic devices likely to be occupied in the studied material. We, therefore, determined the density of the states of our complex based on the structure optimized by DFT. Figure 9 shows the distribution of the density of the states. We observed the presence of a discontinuity which marks

Table 4. Second-Order Perturbation Theory Analysis of Fock Matrix on NBO Basis for a Studied Compound Using b3lyp/6-311g(d,p)

Donor (i)	Type	Acceptor (j)	Type	E(2)[a] (kcal mol^{-1})	E(j) - E(i)[b] (a.u.)	F(i; j)[c] (a.u.)
Fe	LP*	C139	RY*	27.08	0.07	0.103
Fe	LP*	C 140	RY*	21.01	0.18	0.151
Fe	LP*	C 142	RY*	29.11	0.07	0.106
Fe	LP*	C 143	RY*	25.85	0.13	0.139
Fe	LP*	C 151	RY*	36.03	2.03	0.658
N155	LP	C 154	RY*	17.25	1.17	0.127
N155	LP	C144–C154	BD*	11.41	0.95	0.093
Fe1–N151	BD*	Fe	LP*	40.31	0.65	0.253
Fe	LP*	N2	RY*	27.44	1.56	0.502
Fe	LP*	N9	RY*	27.37	1.98	0.564
Fe	LP*	N16	RY*	26.91	2.00	0.563
Fe	LP*	N23	RY*	26.92	1.58	0.501
Fe	LP*	H126	RY*	52.05	0.06	0.134
Fe	LP*	H129	RY*	31.23	0.09	0.127
Fe	LP*	N150	RY*	27.30	1.65	0.516
N2	LP	Fe	LP*	23.38	1.03	0.139
N9	LP	Fe	LP*	24.85	0.26	0.080
N9	LP	Fe	LP*	24.32	1.04	0.142
N16	LP	Fe	LP*	25.99	0.26	0.082
N16	LP	Fe	LP*	24.75	1.04	0.144
N16	LP	Fe	LP*	12.01	0.06	0.025
N23	LP	Fe	LP*	23.70	0.26	0.078
N23	LP	Fe	LP*	23.58	1.04	0.140

the separation between the valence band and the conduction band. Therefore, it can be stated that there is no available state in this gap. Any increase in the energy of an electron in the conduction band leads to an increase in the available states, but to reach the valence band, that electron must lose at least the gap energy of the material.

Natural Bond Orbital (NBO) Analysis

The NBO analysis is an important tool to investigate the intra- and intermolecular bonding and even interaction and provides a suitable basis for analyzing charge transfer or conjugative interaction in molecular systems. Furthermore, NBO analysis, using the virtual and filled orbital spaces, allows researchers to explain the important interactions that enhance the inter- and intra-molecular interactions [37]. The important acceptor and electron donor orbitals and their interaction stabilization energy were analyzed and are reported below. In NBO analysis, the second-order Fock matrix was used to evaluate the donor-acceptor interactions with stabilization energies E(2) $\geq$ 10 kcal mol^{-1}. NBO analysis was carried out using the B3LYP/6-311g(d,p) method. Table 5 shows the selected interactions along with their stabilization energies. In this study, it was chemically important to use the stabilization energy (E2) values in the

objective function to estimate the intramolecular electron transfer.

Based on the data in Table 4, it can be observed that the important interaction of energy in the studied complex was the electron coupling LP*(Fe)→RY*(H126), BD*(Fe–N151)→LP*(Fe), LP*(Fe)→RY*(C151), LP*(Fe)→RY*(H129), LP*(Fe)→RY*(C142), LP*(Fe)→RY*(N2), LP*(Fe)→RY*(N9), LP*(Fe)→RY*(N150), LP*(Fe)→RY*(C139), LP*(Fe)→RY*(N23), and LP*(Fe)→RY*(N16), which stabilized at 52.05, 40.31, 36.03, 31.23, 29.11, 27.44, 27.37, 27.30, 27.08, 26.92, and 26.91 kcal mol^{-1}, respectively. The second-order perturbation theory analysis revealed that the electron transfer in the studied complex was predominant from the Fe lone-pair-antibonding to Rydberg NBOs antibonding for atoms spatially close to it, such as H126, H129, C151, C139, C142, N2, N9, N16, N23, and N150, and from Fe lone-pair-anti bonding to the antiperiplanar Fe–N151 antibonding.

CONCLUSIONS

The structural and absorption spectroscopic properties of the $[Fe^{III}(TMPP)(4\text{-}CNpy)_2]^+$ ion complex (I) were explored theoretically *via* DFT calculations at the B3LYP/6-311G(d,p) level of theory. The optimization of the structure obtained by the B3LYP method with the basis set 6-311G(d,p) provided the closest structural parameters with the experimental X-ray molecular structural data of complex (I). Interestingly, the first-order hyperpolarizability (β_{total}) of (I) (31.4831×10^{-31} esu) was 4 times higher than that of the urea ($\beta_{total} = 7.7289 \times 10^{-31}$ esu), indicating that the title compound is a good candidate for NLO material. Hirshfeld analysis of the studied compound (I) showed that 43.4% of the intermolecular contacts were associated with the H–H contacts, 22% with the contacts between carbon and hydrogen C–H, 8% with the N–H contacts,, and only 1.1% with the π-π stacking (C···C), showing a very weak association. The DFT calculations showed that the HOMO and LUMO orbitals were located around the aromatic cycles surrounding the metal center. The calculated HOMO-LUMO energy gap at the B3LYP/6-311G(d,p) level was found to be 0.9042 eV. This small energy gap value can be explained by the electronic transfer between the *meso*-methoxyphenylporphoyrinato (TMPP) and the 4-cyanopyridine ligands. Furthermore, the theoretical gap energy value (1.911 eV) was obtained from the simulated absorption spectrum of (I). This value, *i.e.* 1.911 eV, was close to the experimental value, *i.e.* 1.71 eV, and the small difference between these two values is probably due to the fact that the theoretical calculations were made in the gaseous state. The electronic properties of complex (I) were obtained from several parameters, such as HOMO and LUMO energies, chemical hardness (η), chemical potential (μ), and electronegativity (χ). The values of these parameters showed that the studied iron(III) porphyrin species behaved as electron donors, had a soft character, and thus were very reactive. Finally, the NBO analysis was performed to explore the interactions and charge transfers among different orbitals of atoms close to the iron metal center and the lone pairs of this cation.

REFERENCES

[1] Milgrom, L. R., The Colours of Life: An Introduction to the Chemistry of Porphyrins and Related Compounds; Oxford University Press: Oxford, UK, **1997**.

[2] Kadish, K. M.; Smith, K. M.; Guilard, R., Applications: Past, Present, and Future, the Porphyrin Handbook; CRC Press: Boca Raton, FL, USA, Volume 6, **2000**.

[3] Schneider, S.; Marles-Wright, J.; Sharp, K. H.; Paoli, M., Diversity and conservation of interactions for binding heme in b-type heme proteins. *Nat. Prod. Rep*. **2007**, *3*, 621-630.

[4] Valicsek, Z.; Horváth, O., Application of the electronic spectra of porphyrins for analytical purposes: The effects of metal ions and structural distortions. *Microchem. J.* **2013**, *107*, 47-62. DOI: https://doi.org/10.1016/j.microc.2012.07.002.

[5] Dini, D.; Calvete, M. J.; Hanack, M., Nonlinear optical materials for the smart filtering of optical radiation. *Chem. Rev.* **2016**, *116*, 13043-13233. DOI: https://doi.org/10.1021/acs.chemrev.6b00033.

[6] Lu, G.; Chen, Y.; Zhang, Y.; Bao, M.; Bian, Y.; Li, X. J., Jiang, Morphology controlled self-assembled nanostructures of sandwich mixed (phthalocyaninato)

(porphyrinato) europium triple-deckers. Effect of hydrogen bonding on tuning the intermolecular interaction, *J. Am. Chem. Soc.* **2008**, *130*, 11623-11630. DOI: httpsdoi.org10.1021ja802493v.

[7] Safo. K.; Gupta, G. P.; Walker, F. A.; Scheidt. W. R., Cytochromes b. control of axial ligand orientation with a "Hindered" porphyrin system, *J. Am. Chem. Soc.* **1991**, *113*, 5497-5510. DOI: httpsdoi.org10.1021ja00015a001.

[8] Haj Hassen, L. B.; Dhifaoui, S.; Rousselin, Y.; Marvaud, V.; Stern, C.; Schulz, C. E.; Nasri, H., New insights on the electronic, magnetic, electric and molecular structure of bis-(4-cyanopyridine) iron(III) complex with the meso-tetrakis (4-methoxyphenyl) porphyrin, *Inorg. Chim. Acta.* **2018**, *486*, 1-30. DOI: https://doi.org/10.1016/j.ica.2018.11.040.

[9] Meyer, A. Y., The size of molecules, *Chem. Soc. Rev.* **1986**, *15*, 449-474. DOI: 10.1039/CS9861500449.

[10] McKinnon, J. J.; Jayatilaka, D.; Spackman, M. A., Towards quantitative analysis of intermolecular interactions with Hirshfeld surfaces, *Chem. Commun*. **2007**, *37*, 3814-3816. DOI: 10.1039B704980C.

[11] Delgado, G. E.; Liew, S. M.; Jamalis, J.; Cisterna, J.; Cardenas, A.; Brito, I., Structural characterization and Hirshfeld surface analysis of the pyrazoline 1-(3-(4-iodophenyl)-5-(3-methylthiophen-2-yl)-4,5-dihydro-1H-pyrazol-1-yl) ethan-1-one, *J. Mol. Struct.* **2020**, *1210*, 8044. DOI: 10.1016j.molstruc.2020.128044.

[12] Wolff, S. K.; Grimwood, D. J.; McKinnon, J. J.; Turner, M. J.; Jayatilleka, D.; Spackman, M. A.; Crystal Explorer 3.1, University of Western Australia, Crawley, Western Australia, **2013**, pp. 2005-2013.

[13] Dhifaoui, S.; Hajji, M.; Nasri, S.; Guerfel, T.; Daran, J. C.; Nasri, H.; A new high-spin iron(III) bis(aqua) complex with the mesotetra(*para*-chlorophenyl) porphyrin: X-ray crystallography, Hirshfeld surface analysis, magnetic, EPR and electrochemical properties, *Res. Chem. Intermed.* **2018**, *44*, 7259-7276. DOI: 10.1007s11164-018-3555-1.

[14] Becke, A. D., Density-functional exchange-energy approximation with correct asymptotic behavior, *Phys. Rev. a*, **1988**, *38*, 3098-3100. DOI: 10.1103/PhysRevA.38.3098.

[15] Gerber, I. C.; Angyan, J. G., Hybrid functional with separated range, *Chem. Phys. Lett.* **2005**, *415*, 100-105. DOI: httpsdoi.org10.10631.447079.

[16] Gaussian 09, Revision D.01, Frisch, M. J.; Trucks, G. W.; Schlegel, H. B.; Scuseria, G. E.; Robb, M. A.; Cheeseman, J. R; Scalmani, G.; Barone,V.; Mennucci, B.; Petersson, G. A.; Nakatsuji, H.; Caricato, M.; Li, X.; Hratchian, H. P.; Izmaylov, A. F.; Bloino, J.; Zheng, G.; Sonnenberg, J. L.; Hada, M.; Ehara, M.; Toyota, K.; Fukuda, R.; Hasegawa, J.; Ishida, M.; Nakajima, T.; Honda, Y.; Kitao, O.; Nakai, H.; Vreven, T.; Montgomery, J. A.; Peralta, J. E.; Ogliaro, F.; Bearpark, M.; Heyd, J. J.; Brothers, E.; Kudin, K. N.; Staroverov, V. N.; Kobayashi, R.; Normand, J.; Raghavachari, K.; Rendell, A.; Burant, J. C.; Iyengar, S. S.; Tomasi, J.; Cossi, M.; Rega, N.; Millam, J. M.; Klene, M.; Knox, J. E.; Cross, J. B.; Bakken, V.; Adamo, C.; Jaramillo, J.; Gomperts, R.; Stratmann, R. E.; Yazyev, O.; Austin, A. J.; Cammi, R.; Pomelli, C.; Ochterski, J. W.; Martin, R. L.; Morokuma, K.; Zakrzewski, V. G.; Voth, P.; Salvador, J. J.; Dannenberg, S.; Dapprich, A. D.; Daniels, Ö.; Farkas, J. B.; Foresman, J. V., Ortiz, Cioslowski G. A. J.; Fox, D. J., Gaussian, Inc., Wallingford CT, **2009**.

[17] Yanai, T.; Tew, D. P.; Handy, N. C., A new hybrid exchange-correlation functional using the Coulomb-attenuating method (CAM-B3LYP), *Chem. Phys. Lett.* **2004**, *393*, 51-57. DOI: 10.1016/j.cplett.2004.06.011

[18] Chitrambalam, S.; Manimaran, D.; Hubert, J. I.; Rastogi, V. K.; Hassan, U. L., Synthesis, Hirshfeld surface analysis, laser damage threshold, third-order nonlinear optical property and DFT computation studies of Dichlorobis (DL-valine) zinc(II): A spectroscopic approach, *Opt. Mater*. **2018**, *75*, 285-296. DOI: httpsdoi.org10.1016j.optmat.2017.10.003.

[19] Andraud, C.; Brotin, T.; Garcin, C.; Pell, F.; Coldner, P.; Bigot, B.; Collet, A., Theoretical and experimental investigations of the nonlinear optical properties of vanillin, polyenovanillin, and bisvanillin derivatives. *J. Am. Chem. Soc.* **1994**, *116*, 2094-2102. DOI: doi.org/10.1021/ja00084a055.

[20] Geskin, V. M.; Lambert, C.; Brédas, J. L.; Origin of high second- and third-order nonlinear optical response in ammonio/borato diphenylpolyene

zwitterions: The remarkable role of polarized aromatic groups, *J. Am. Chem. Soc.* **2003**, *125*, 15651-15658. DOI: doi.org/10.1021/ja035862.

[21] Alyar, H.; Alyar, S., Electronic and nonlinear optical (NLO) properties of fluorophenylpyridines, *IJISET*. **2017**, *4*, 76-84.

[22] Kacimi, R.; Abram, T.; Bejjit, L.; Bouachrine, M., New organic materiel based on benzothiadiazole for Photovoltaic application Solar Cells, *Mater. Today. Proc.* **2019**, *13*, 1188-1196. DOI: doi.org10.1016j.matpr.2019.04.087.

[23] Bouachrine, M.; Benaqqa, O.; Toufik, H.; Hamidi, M.; Lère-Porte, J. P.; Serein-Spirau, F.; Amine, A., Experimental and quantum chemical investigation of new electroluminescent material based on thiophene, phenylene and antracene, *An. Univ. Bucuresti. Chimie* **2010**, *19*, 35-44.

[24] Sinha, L.; Prasad, O. V.; Narayan, S. R., Shukla, R., FT-IR spectroscopic analysis and first-order hyperpolarizability of 3-benzoyl-5-chlorouracil by first principles, *Mol. Simu*. **2011**, *37*, 153-163. DOI: 10.108008927022.2010.533273.

[25] Lewis, D. F. V.; Ioannides, C.; Parke, D. V., Interaction of a series of nitriles with the alcohol-inducible isoform of P450: Computer analysis of structure-activity relationships, *XENOBIOTICA*, **1994**, *44*, 201-408. DOI: 10.31090049825940904324 3.

[26] Hocking, R. K.; Wasinger, E. C.; Yan, Y. L.; Walker, F. A.; Hodgson, K. O.; Hedman, B.; Solomon, E. I., Fe L-edge X-ray absorption spectroscopy of low-spin heme relative to non-heme Fe complexes: delocalization of Fe d electrons into the porphyrin ligand, *J. Am. Chem. Soc.* **2007**, *129*, 113-125.DOI: 10.1021/ja065627h.

[27] Conradie, J.; Ghosh, A., Do the one-electron oxidized derivatives of some six-coordinate low-spin iron(III) porphyrins feature strong metal-ligand ferromagnetic coupling. *J. Phys. Chem. B*. **2003**, *107*, 6486-6490. DOI: 10.1021/jp030354.

[28] Parr, R. G.; Donnelly, R. A.; Levy, M; Palke, W. E., Electronegativity: The density functional viewpoint, *J. Chem. Phys.* **1978**, *68*, 3801-3807. DOI: 10.1063/1.436185.

[29] Pearson, R. G., Absolute electronegativity and hardness correlated with molecular orbital theory, *Proc. Nati. Acad. Sci. USA.* **1986**, *83*, 8440-8441. DOI: 10.1073pnas.83.22.8440.

[30] Parthasarathi, R.; Subramanian, V.; Chattaraj, P. K., Effect of electric field on the global and local reactivity indices, *Chem. Phys. Lett*. **2003**, *382*, 48-56. DOI: 10.1016j.cplett.2003.09.160.

[31] Schildcrout, S. M.; PearsonStafford, R. G., F. E., Ionization potentials of tris (β-diketonate) metal(III) complexes and koopmans'theorem, *J. Am. Chem. Soc.* **1968**, 4006-4010. DOI: 10.1021ja01017a017.

[32] Pearson, R. G., Absolute electronegativity and hardness: Application to inorganic chemistry, *Inorg. Chem.* **1988**, *27*, 734-740. DOI: 10.1021ic00277a030.

[33] Senet, P., Chemical hardnesses of atoms and molecules from frontier orbitals, *Chem. Phys. Lett.* **1997**, *275*, 527-532. DOI: 10.1016S0009-2614(97)00799-9.

[34] Bhawsar, J.; Jain, P.; Valladares-Cisneros, M. G.; Cuevas, A. C. M.; Bhawsar, R., Quantum chemical assessment of two natural compounds: Vasicine and vasicinone as green corrosion inhibitors. *Int. J. Electrochem. Sci.* **2018**, *13*, 3200-3209. DOI: 10.20964/2018.04.57.

[35] Gasteiger, J.; Li, X. I.; Rudolpb, C.; Sadowski, J.; Zupan, J., Representation of molecular electrostatic potentials by topological feature maps, *J. Am. Chem. Soc.* **1994**, *116*, 4608-4620. DOI: https:10.1021/ja00090a009.

[36] Lan, M.; Zhao, H.; Yuan, H.; Jiang, C.; Zuo, S.; Jiang. Y. I., Absorption and EPR spectra of some porphyrins and metalloporphyrins, *Dyes and Pigments,* **2007**, *74*, 357-362. DOI: 10.1016j.dyepig.2006.02.018.

[37] Wei, L.; She, Y.; Yu, Y.; Yao, X.; Zhang. S., *J. Mol. Model.* **2012**, *18*, 2483-2491. DOI: 10.1007/s00894-011-1279-x.